Water Air Soil Pollut (2019) 230: 243
https://doi.org/10.1007/s11270-019-4301-z

Equilibrium and Kinetic Study of Ammonium Sorption by *Raphia farinifera*

Paweł Staroń · Paulina Sorys · Jarosław Chwastowski

Received: 17 May 2019 / Accepted: 25 September 2019 / Published online: 24 October 2019

Abstract The study investigated the sorption capacity of biosorbent-*raphia* sp. against ammonia. *Raphia* fibers were used without and with the modification of its surface with NaCl, $NaNO_3$, and K_2SO_4. The data was analyzed in the state of equilibrium using four isotherm models such as Langmuir, Freudlich, Temkin, and Dubinin-Radushkevich. The equilibrium of ammonia sorption for all studied systems was best described by the Freudlich isotherm model. On its basis, it can be assumed that the studied process is of chemical nature, which results from the value of the coefficient $1/n < 1$. In order to confirm the sorption mechanism, analysis of the kinetics of the ammonia sorption process on *raphia* fibers was performed. Four kinetic models of sorption were calculated: pseudo-first-order model, pseudo-second-order model, Elovich model, and Webber-Morris intermolecular diffusion model. The sorption kinetics of the modeled ammonia waste were carried out using unmodified palm fibers and all kinds of surface modification. This process was best described by the pseudo-second-order sorption model, which can be considered as a confirmation of the chemical nature of ammonia sorption on *raphia* sp. fibers.

Keywords Ammonium · Biosobent · *Raphia* · Sorption · Palm

P. Staroń (✉) · P. Sorys · J. Chwastowski
Department of Engineering and Chemical Technology, Cracow University of Technology, 24 Warszawska St, 31-155 Cracow, Poland
e-mail: pstaron@chemia.pk.edu.pl

1 Introduction

Ammonia is part of the natural cycle of nitrogen circulation in nature; however, an artificial source of ammonia in the case of water pollution causes excessive eutrophication and algal bloom, which leads to disturbance of the balance of the aquatic ecosystem. Increased ammonia concentration in water has a particularly negative effect on fish development causing gill damage, hyperplasia, and significant reduction of growth rate (Cui et al. 2016; Conley et al. 2009; Długosz and Banach 2018b).

Ammonia occurs naturally in the environment mainly in the form of ammonium salts. It is released in the volatile NH_3 form mainly due to decomposition of nitrogen-containing organic substances and as a result of volcanic activity. Another natural source of ammonia is electrical discharges that arise in the atmosphere that allow the reaction of oxygen with molecular nitrogen. As a result of the reaction, ammonia and its oxidation products are formed, which subsequently react with each other to form ammonium nitrate (V) and ammonium nitrate (III). Part of the nitrates produced according to this mechanism reaches the earth's surface, from which they are absorbed by plants, because they contain nitrogen in a form that is available to them (Appl 1999). Ammonia is widely used in the production of fertilizers and animal feed as well as in the production of fibers, plastics, explosives, paper, and rubber (Šiljeg et al. 2010). The largest uncontrolled emission of ammonia to the environment comes from livestock

Table 1 Modification of the surface of *raphia* fibers

L.p.	Modification agent	Concentration [mol/dm^3]	Modification time [h]
1	NaCl	1	3
2			54
3	$NaNO_3$	1	16
4	K_2SO_4	0.5	16

breeding, manure management, and fertilizer application. In case of insufficient ventilation of the breeding rooms, respiratory diseases appear in the animals, which results in a decrease in the production of milk, meat, and eggs (Alberdi et al. 2016; Henry and Aherne 2014). Currently used techniques of removing ammonia from water and wastewater are biological method using activated sludge to remove nitrogen compounds in sewage treatment plants, division in the air stream, and ion exchange carried out in columns with zeolite filling, chemical precipitation, ion exchange, membrane separation (Zhang et al. 2009; Jorgensen and Weatherley 2003; Shalini and Joseph 2012; Huang et al. 2015).

An alternative to commonly used techniques is sorption of ammonia on a properly selected sorbent. The sorbent should meet a number of requirements: be easily accessible and durable both mechanically and chemically, have high sorption capacity and high affinity for analyte, and enable recycling by lowering process costs (Veliscek-Carolan et al. 2019; Azimi et al. 2019; Bhardwaj and Bhaskarwar 2018; Hu et al. 2019).

The aim of the research was to check the possibility of using *raphia* fibers to remove ammonia from aqueous solutions. *Raphia* fibers belong to organic materials containing lignin and cellulose in their composition (Xu et al. 2018). The ammonia removal process was carried out in the batch system, allowing to obtain information about the maximum sorption capacity of the material in relation to the analyzed analyte. *Raphia* fibers have also been subjected to chemical modification to improve its sorption capacity. Obtained results of the research allowed for adaptation of the sorption isotherm and determination of sorption kinetics allowing to obtain basic information on the mechanisms of ammonia sorption on *raphia* fibers. The solute removal rate controlling residence time in the liquid-solid interface is expressed by the sorption kinetics. One of the most important factors in the designing of the sorption system is the sorption rate, because the kinetics determine the reactor dimensions what is connected with the solute residence time. In order to understand the sorption kinetics, various models have been studied.

Pseudo-first-order and pseudo-second-order kinetic models are the most used to study metal sorption kinetics to solids (Veneu et al. 2018; Guo and Wang 2019).

2 Materials and Methods

2.1 Materials

The research involved the use of *raphia* fiber (*Raphia farinifera*) purchased in the commercial store. *Raphia* test was prepared by cutting fibers into pieces with the length of approx. 3–4 mm and a five-fold rinsing in demineralized water. One rinse cycle lasted 10–15 min. The aim of the washing was to purify and unify the research material. The most favorable purification conditions were obtained by mixing approx. 20 g of *raphia* in approx. 1.5 dm^3 of demineralized water. All used solutions were prepared in distilled water. Reagents used in the tests were purchased from Sigma-Aldrich and were characterized by analytical purity.

2.2 Surface Modification

The process of surface modification of the *raphia* fibers was carried out using aqueous salt solutions according to Table 1. Substitution of silicon by aluminum atoms in the crystal backbone leads to an additional negative charge balanced by surrounding counterions (such as Na+, K+, Ca2+, and Mg2+), and these counterions are easily exchanged by other surrounding cations in contact solution. To 10 g of *raphia*, 100 cm^3 of the modifying solution was added and mixed for a limited time.

According to the fundamental of ion exchange between solid and liquid phases, the ion exchange process between zeolite frame and aqueous ammonium solution can be expressed by the following equation.

$$Rf–Me^{n+} + nNH_4{}^{+} = Rf–nNH_4{}^{+} + Me^{n+}$$

Table 2 Isotherm model equations

No.		Equation	Reference
Isotherm models			
1	*Langmuir*	$\frac{C_e}{q_e} = \frac{C_e}{q_{max}} + \frac{1}{b \cdot q_{max}}$	(Azizian et al. 2018)
2	*Freundlich*	$logq_e = logK_f + \frac{1}{n} logC_e$	(Coles and Yong 2002)
3	*Temkin*	$q_e = BlnK_t + BlnC_e$ $B = \frac{RT}{b_t}$	(Araújo et al. 2018)
4	*Dubinin-Radushkevich*	$lnq_e = ln\, q_d - (B_d\varepsilon^2)$ $\varepsilon = RTln\left(1 + \frac{1}{C_e}\right)$	(Abdelnaeim et al. 2016)

where Ze and M represent the zeolite and the loosely held cations in zeolite, respectively, and *n* is the number of electric charge (Lin et al. 2013).

2.3 Sorption Process

The ammonia sorption process was carried out in a batch dynamic mixing system. The variable parameters of the sorption process were the concentration of ammonia and the time of running the process. The sorption process was carried out in a 60-cm^3 PP beaker; 0.5 g of previously prepared *raphia* fibers and 40 cm^3 of ammonia solution were used each time. Five concentrations of model solutions were determined for which further tests were conducted: 1, 3, 5, 7, and 9 mmol/dm^3. The sorption time was 0.5, 1, 2, 4, 6, 10, and 15 min. After the sorption process, the solutions were filtered, and then, the ammonia content was determined by titration.

2.4 Physicochemical Characteristics

The analysis of the elemental composition of *raphia* fibers before and after the sorption process was carried out using the compact energy-dispersive spectrometer X-ray PW4025/00 MiniPal by PANalytical B.V. A specific surface area test was carried out using a ASAP 2010 deaerator station. Before measurement, samples were dried in a helium atmosphere at 110 °C for 8 h, then under vacuum at 100 °C and 0.001 Tor for 8 h. Surface analysis was performed with an LEO 1430 VP scanning electron microscope. SEM photomicrographs were taken on Hitachi TM-3000 equipped with an X-ray micro analyzer EDS. CHN analysis was performed using the Perkin Elmer Type 2400 CHN analyzer. Fourier transform infrared spectroscopy was performed on a Scimitar Series FTS 2000 from Digilab.

Table 3 Kinetic model equations

No.		Equation	Reference
1	*Pseudo-first order*	$\log(q_e - q_t) = log_{qe} - \frac{k_l}{2.303} t$	(Długosz and Banach 2018a)
2	*Pseudo-second order*	$\frac{t}{q_t} = \frac{1}{k_2 q_e^2} + \frac{t}{q_e}$	(Simonin 2016)
3	*Weber-Morris*	$q_t = k_{id} t^{0.5} + I$	(Zhu et al. 2016)
4	*Elovich*	$q_t = \frac{1}{\beta}\ln(\alpha\beta) + \frac{1}{\beta}\ln(t)$	(Inyang et al. 2016)

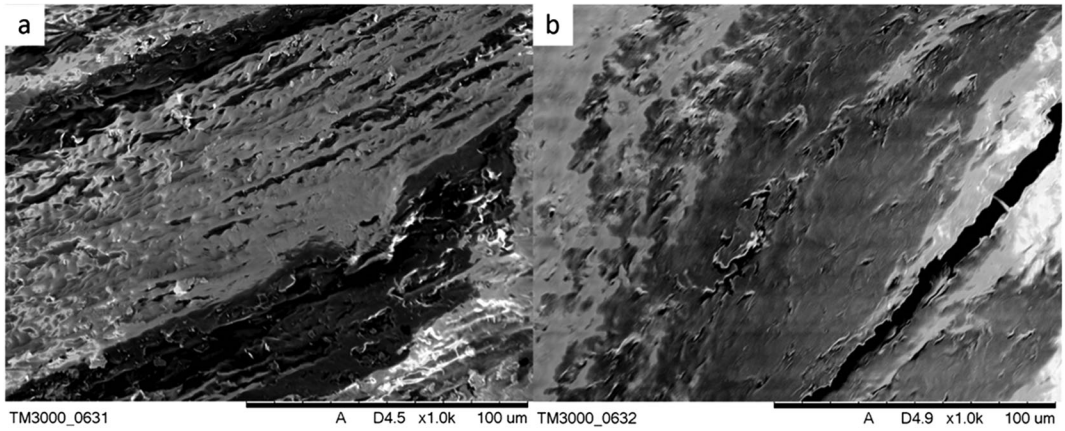

Fig. 1 SEM micrograph of *raphia* fiber: **a** before sorption, **b** after sorption

2.5 Equilibrium Studies

The equilibrium parameters of ammonia sorption on *raphia* fibers were modeled on the basis of the isotherms: Langmuir, Freundlich, Temkin, and Dubinin-Radushkevich isotherms (Table 2).

2.6 Kinetic Models

Investigating the influence of the sorption time allows to determine the mechanisms of the sorption process. In order to determine the effect of contact time of *raphia* fibers (before and after modification), sorption capacity of *raphia* fiber in relation to ammonia at different times at various initial concentrations was investigated. Table 3 presents the kinetic models used.

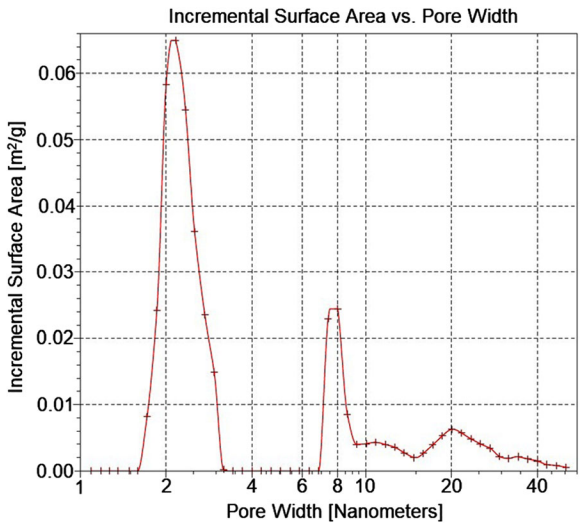

Fig. 2 Porosity graph of coconut fiber

3 Result and Discussion

3.1 Materials Characterization

The *raphia* fibers prior to the sorption process have a heterogeneous structure with a fibrous structure (Fig. 1a), whereas the structure of *raphia* fibers after the sorption process (unmodified—UM) was characterized by a structure with greater homogeneity (Fig. 1b). BET analysis showed that the specific surface area of *raphia* fibers had a specific surface area of 1.079 m^2/g; moreover, the fiber surface is characterized by a mesoporous structure (Fig. 2).

Analysis of the XRF spectrum of *raphia* without surface modification and after its modification showed the presence of nine elements. The material was marked

Table 4 Elemental composition of *raphia* without modification and modification

Element	Content [%]			
	Without modification	$NaNO_3$	K_2SO_4	NaCl 54 h
Si	17	26	15	5
P	15	27	10	18
S	6	15	5	6
K	10	–	52	–
Ca	44	24	15	60
Ti	1	–	–	–
Mn	2	1	1	6
Fe	4	6	3	5
Ni	1	1	–	1
Al	3	1	–	1

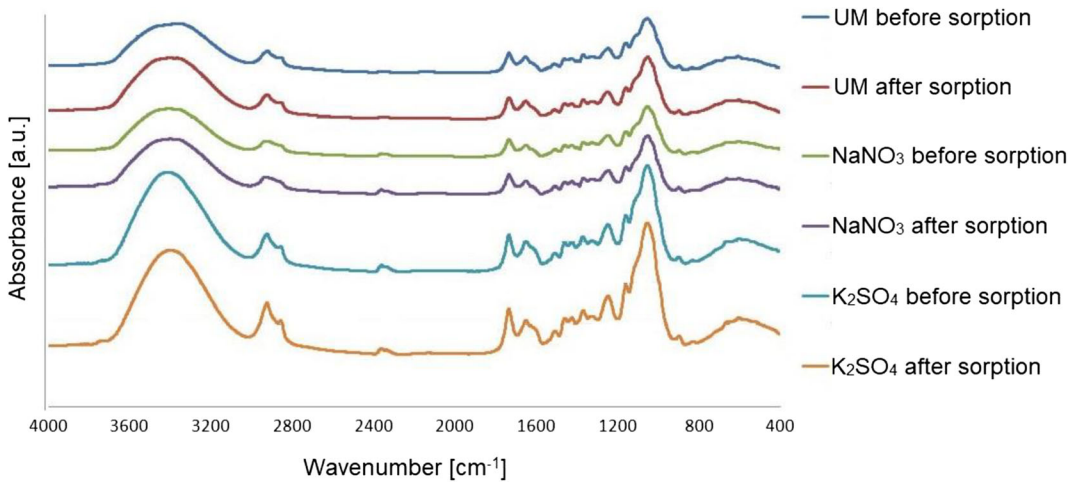

Fig. 3 *Raphia* IR interferogram

with the highest content of calcium, silicon, phosphorus, and potassium. In addition, based on elemental analysis of CHN, it was found that the content was equal to C: 46.04%, H: 6.18%, and N: 0.77%. These values are similar to those obtained by other researchers during analyses of organic materials (Bispo et al. 2018; Chwastowski et al. 2017).

The results of the semi-quantitative (non-patterned) analysis are shown in Table 4. The XRF technique allows the determination of elements heavier than sodium (MNa = 22.99 g/mol). *Raphia* as an organic substance consists mainly of carbon (MC = 12.01 g/mol), which is why the presented percentage composition of elements present in the structure of *raphia* is inflated and is illustrative (Hunt and Speakman 2015).

Raphia without surface modification from the elements detected by the XRF technique contains the most calcium (44%). Silicon, phosphorus, and potassium are present in a smaller amount with a percentage of 17, 15, and 10%, respectively. The analysis showed the presence of sulfur, titanium, manganese, iron, and nickel.

$NaNO_3$ modification caused a decrease in the content of calcium by 45% and potassium by 100%, which resulted in an increase in the percentage of silicon, phosphorus, and sulfur.

Percentages of calcium, silicon, phosphorus, and potassium are similar and amount to 24, 26, 27, and 15%, respectively.

Modification of K_2SO_4 caused an increase in the potassium content by 420%, resulting in a 66% decrease in calcium content. The element with the highest percentage share in this sample is potassium—52%.

The NaCl modification reduced the silicon content by 71% and potassium by 100%, resulting in an increase in the percentage of calcium by 36%. The element with the largest percentage share in this sample is calcium—60%.

Figure 3 shows the IR interferogram of the *raphia* without surface modification and with the modified surface made before and after the sorption process. In the range of 3600–3200 cm^{-1}, there is an area characteristic for the vibration of the hydroxyl group (–OH). The peak at 1050 cm^{-1} corresponds to the amino group (–NH), peak 1650 cm^{-1} carbonyl group (–COOH), peak 2900 cm^{-1} group $–CH_2–$ (Staroń et al. 2017). The peak at 2360 cm^{-1} is the result of the presence of CO_2. With each measurement, the intensity of this peak increases as opening the measuring chamber of the spectrometer to place the sample caused the diffusion of CO_2 from the air in the laboratory inside the device. On the presented interferogram, there are no changes in the peaks for the modified raphia compared to the unmodified material, what results from the modifying substances used. Salts change the acidic and basic surface groups, which changes only the FTIR intensity not spectrum. In addition, slight shifts in the spectrum after the sorption process can be observed, which is possible with overlapping of the peaks associated with NH_4^+ groups (Petit et al. 2006).

One of the most important factors affecting the degree of removal of ammonia from the solution is the

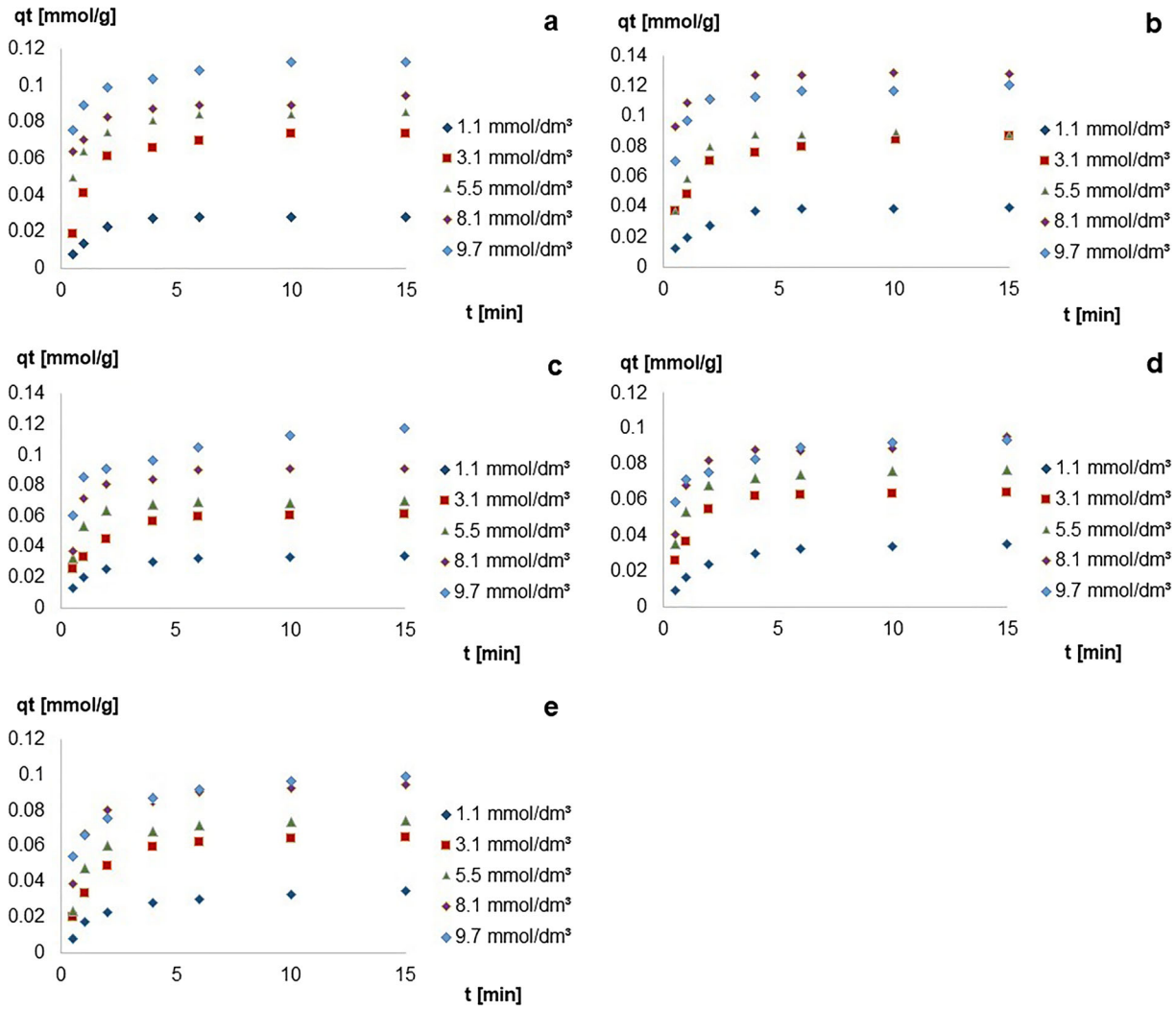

Fig. 4 Sorption of ammonium on *raphia* fiber over time at different initial concentrations, modification: **a** without modification, **b** NaCl 3 h, **c** NaCl 54 h, **d** $NaNO_3$ 17 h, **e** K_2SO_4 16 h

contact time of the solution with the sorption bed. In Fig. 4, it is observed that with sorption time prolongation, the sorption capacity qt of *raphia* increases, up to the limit of 0.11 mmol/g for unmodified material, 0.13 mmol/g for modified with NaCl, 0.10 mmol/g for $NaNO_3$, and 0.1 mmol/g for K_2SO_4. The highest sorption rate occurs at the beginning of the process until about the second minute. Then, it decreases, until reaching the sixth minute of sorption equilibrium between the content of ammonia in the solution and sorbated by *raphia*.

Figure 5 shows the degree of removal (R_e) of ammonia at the equilibrium for individual concentrations of initial ammonia in the model wastewater. The lower the initial concentration of ammonia, the higher the ammonia removal in equilibrium state R_e. The highest removal rate was obtained using *raphia* modified with NaCl for 3 h. Increase of sorption with unmodified *raphia* surface by NaCl modification for 3 h occurs only at initial ammonia concentrations below 3 mmol/dm^3. The lower the initial concentration of ammonia, the higher the ammonia removal in equilibrium state R_e. The highest removal rate was obtained using *raphia* modified with NaCl for 3 h. Increase in sorption with modified *raphia* by NaCl for 3 h occurs only at initial ammonia concentrations below 3 mmol/dm^3. The modification of *raphia* surface with NaCl for 54 h, $NaNO_3$, and

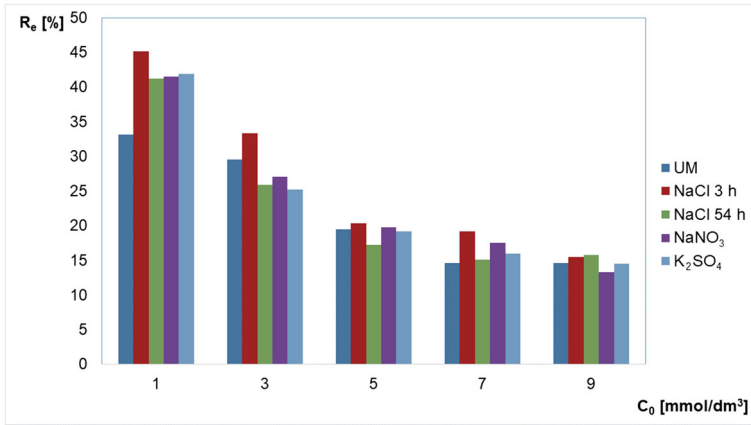

Fig. 5 The degree of removal (R_e) of ammonia on the surface of *raphia*

K_2SO_4 increases the sorption of ammonia only for a solution 1 mmol/dm^3. In other cases, modification of the sorbent surface did not improve the sorption capacity of *raphia* in relation to ammonia. The modification of *raphia* surface with NaCl for 54 h, $NaNO_3$, and K_2SO_4 increases the sorption of ammonia only for a solution of 1 mmol/dm^3. In other cases, modification of the sorbent surface did not improve the sorption capacity of *raphia* in relation to ammonia.

Table 5 Equations and parameters of the sorption equilibrium for individual sorbents

Isotherm	Modification	Isotherm equation	R^2	Qmax [mmol/g]	K_L [L/mmol]
Langmuir	UM	$y = 7.15x + 18.48$	0.9653	0.14	0.39
	NaCl 3 h	$y = 6.67x + 12.57$	0.9510	0.15	0.53
	NaCl 54 h	$y = 7.06x + 20.16$	0.8754	0.14	0.35
	NaNO3 17 h	$y = 8.76x + 13.76$	0.9870	0.11	0.64
	K_2SO_4 16 h	$y = 8.16x + 16.34$	0.9785	0.12	0.50
	Modification	Isotherm equation	R^2	K_F ($mg^{-1(1/n)}(dm^3)^{1/n}g^{-1}$)	1/n
Freudlich	UM	$y = 0.52x - 1.42$	0.9248	0.038	0.52
	NaCl 3 h	$y = 0.43x - 1.28$	0.9355	0.053	0.43
	NaCl 54 h	$y = 0.44x - 1.38$	0.9634	0.042	0.44
	$NaNO_3$ 17 h	$y = 0.41x - 1.36$	0.9788	0.044	0.41
	K_2SO_4 16 h	$y = 0.42x - 1.37$	0.9972	0.043	0.42
	Modification	Isotherm equation	R^2	K_t [dm^3/g]	B
Temkin	UM	$y = 0.072x + 0.042$	0.9605	1.79	0.072
	NaCl 3 h	$y = 0.073x + 0.056$	0.9207	2.15	0.073
	NaCl 54 h	$y = 0.066x + 0.042$	0.8706	1.90	0.066
	$NaNO_3$ 17 h	$y = 0.057x + 0.046$	0.9737	2.25	0.057
	K_2SO_4 16 h	$y = 0.059x + 0.044$	0.9731	2.13	0.059
	Modification	Isotherm equation	R^2	E (J/mol)	q_d (mmol/g)
Dubinin-Radushkevich	UM	$y = -0.044x - 1.46$	0.9575	3.38	0.23
	NaCl 3 h	$y = -0.035x - 1.50$	0.9499	3.79	0.22
	NaCl 54 h	$y = -0.035x - 1.70$	0.9383	3.77	0.18
	$NaNO_3$ 17 h	$y = -0.033 - 1.77$	0.9892	3.91	0.17
	K_2SO_4 16 h	$y = -0.33x - 1.76$	0.9897	3.87	0.17

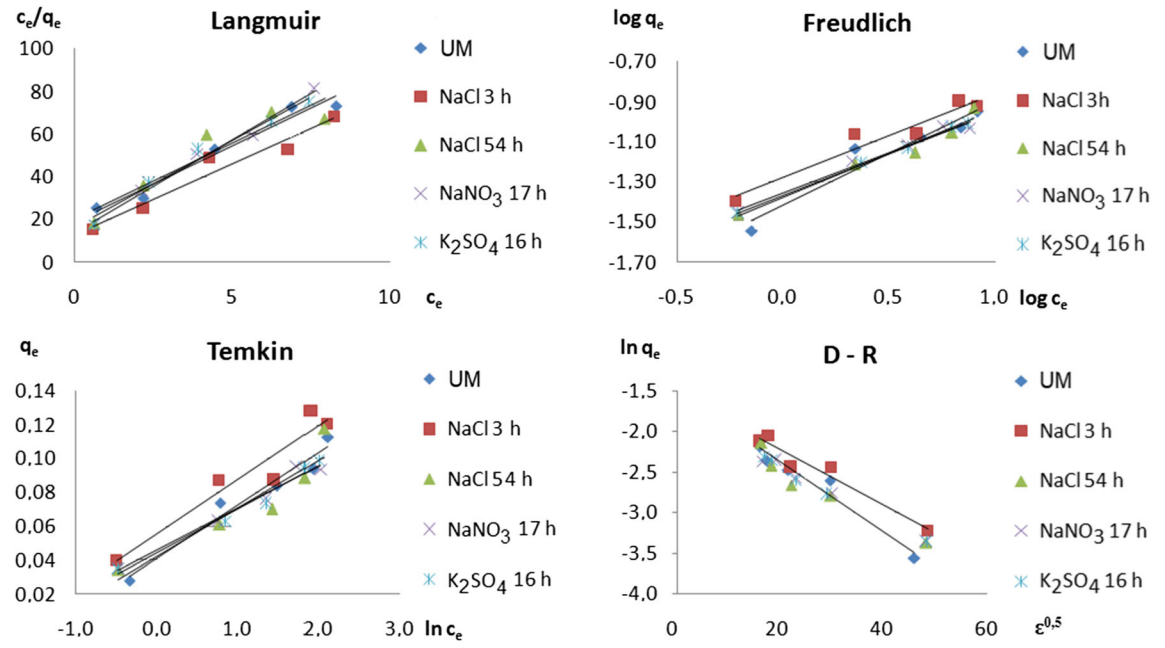

Fig. 6 Isotherms of ammonia sorption on *raphia*

3.2 Equilibrium Studies

In order to select a model of ammonia sorption equilibrium on *raphia*, the obtained data were analyzed in equilibrium. Isotherm equations and determined isothermal parameters for individual sorbents are presented in Table 5. In the case of *raphia* without surface modification and modified NaCl for 3 h, the best fit to the measurement data was obtained for the Langmuir model (determination coefficient, respectively: $R^2 = 0.9653$, $R^2 = 0.9510$). The sorption equilibrium of *raphia*-modified surface for 54 h with NaCl and K_2SO_4 is best described by the Freundlich model ($R^2 = 0.9634$ and $R^2 = 0.9972$, respectively) and *raphia* modified with the $NaNO_3$-D-R isotherm ($R^2 = 0.9892$).

Based on the Langmuir equation, one can determine the R_L constant ($R_L = \frac{1}{1+K_F C_0}$), from which it can be concluded whether the conditions of the sorption process are favorable ($R_L = 0$: sorption is reversible, $0 < R_L < 1$: sorption conditions are preferred, $R_L = 1$: the nature of the sorption is linear, $R_L > 1$: the sorption conditions are unfavorable) (Milonji et al. 2002).

For all initial ammonia concentrations, the K_L parameter ranges from 0 to 1. On this basis, it can be assumed that sorption conditions of ammonia on *raphia* are favorable.

Figure 6 presents graphical representations of sorption equilibrium models for all types of sorbent. For individual cases, the measurement data deviate from the linearity: NaCl-modified *raphia* for 3 h and NaCl for 54 h in the Temkin model, *raphia* modified with NaCl for 54 h in the Langmuir model. In other cases, the R^2 determination coefficients are above 0.9249. On this basis, it can be concluded that all four models of sorption equilibrium predict the equilibrium of sorption of ammonia on *raphia* in a reliable manner. This may be due to the concentration of ammonia in the modeled waste at the millimole level.

3.3 Sorption Kinetics

In order to confirm the sorption mechanism, an analysis of kinetics of ammonia sorption on *raphia* was performed. Four kinetic models of sorption were calculated: the pseudo-first-order model, the pseudo-second-order model, the Elovich model, and the intramolecular diffusion model. Table 6 presents sorption parameters of individual kinetic models for a given sorbent: unmodified *raphia* and four surface modification.

Compared with natural raphia fibers, the modified material showed higher ammonium adsorption

Table 6 Kinetic parameters of different sorption models of ammonium

Kinetic model	Ammonium concentration C_o (mmol/dm^3)				
	1	3	5	7	9
UM					
Pseudo-first-order rate model					
q_e	0.0139	0.0414	0.0262	0.0211	0.0541
k1	0.420	0.327	0.353	0.243	0.541
R^2	0.7971	0.9077	0.8661	0.7840	0.9381
Pseudo-second-order rate model					
q_e	0.030	0.079	0.087	0.096	0.116
k2	35.43	12.17	32.63	35.31	25.91
R^2	0.9955	0.9964	0.9999	0.9997	0.9998
Elovich model					
α	0.07	0.20	4.42	33.88	34.57
β	162.07	65.99	97.06	112.38	92.14
R^2	0.8718	0.8716	0.8958	0.8720	0.9484
Intra-particle diffusion model					
I	0.0100	0.0267	0.0539	0.0659	0.0779
K_{id}	0.0059	0.0145	0.0099	0.0086	0.0107
R^2	0.6890	0.6996	0.7192	0.7111	0.8104
NaCl 3 h					
Pseudo-first-order rate model					
q_e	0.0271	0.0428	0.0428	0.0374	0.0256
k1	0.3756	0.2822	0.5358	0.6087	0.2355
R^2	0.9795	0.9394	0.9649	0.8942	0.6791
Pseudo-second-order rate model					
q_e	0.0430	0.0911	0.0912	0.1307	0.1222
k2	21.15	14.16	22.96	36.67	27.51
R^2	0.9992	0.9996	0.9991	0.9999	0.9996
Elovich model					
α	0.09	0.48	0.81	291.30	16.20
β	118.90	67.43	70.23	96.87	77.92
R^2	0.9543	0.9349	0.8245	0.9049	0.7850
Intra-particle diffusion model					
I	0.0127	0.0385	0.0465	0.0970	0.0817
K_{id}	0.0083	0.0146	0.0133	0.00999	0.01197
R^2	0.8155	0.7945	0.6296	0.7438	0.5990
NaCl 54 h					
Pseudo-first-order rate model					
q_e	0.0197	0.0429	0.0203	0.0277	0.0507
k1	0.3304	0.5210	0.3377	0.3430	0.2278
R^2	0.9429	0.9851	0.7934	0.8074	0.9512
Pseudo-second-order rate model					
q_e	0.0365	0.0650	0.0719	0.0930	0.1218
k2	30.57	19.77	36.02	24.83	11.40
R^2	0.9993	0.9989	0.9995	0.9990	0.9972
Elovich model					
α	0.1315	0.2430	1.4628	1.4096	2.4320
β	157.33	86.59	102.13	75.55	65.61
R^2	0.9581	0.9357	0.7895	0.7502	0.9367
Intra-particle diffusion model					
I	0.0135	0.0251	0.0415	0.0518	0.0626
K_{id}	0.0063	0.0113	0.0091	0.0122	0.0156
R^2	0.8332	0.7896	0.5947	0.5601	0.8594
$NaNO_3$ 17 h					
Pseudo-first-order rate model					
q_e	0.0239	0.0204	0.0235	0.0270	0.0332
k1	0.3393	0.3438	0.3082	0.1553	0.2784
R^2	0.9686	0.6188	0.7970	0.5042	0.9857
Pseudo-second-order rate model					
q_e	0.0383	0.0658	0.0786	0.0967	0.0955
k2	20.21	26.92	29.13	18.74	22.28
R^2	0.9986	0.9986	0.9995	0.9967	0.9993
Elovich model					
α	0.0665	0.3894	1.1498	1.4930	10.5558
β	127.97	90.64	89.15	74.96	102.16
R^2	0.9528	0.8479	0.8156	0.7766	0.9722
Intra-particle diffusion model					
I	0.0098	0.0305	0.0432	0.0523	0.0591
K_{id}	0.0077	0.0104	0.0105	0.0126	0.0099
R^2	0.8092	0.6611	0.6237	0.6035	0.8799
K_2SO_4 16 h					
Pseudo-first-order rate model					
q_e	0.0234	0.0443	0.0352	0.0347	0.0337
k1	0.266	0.661	0.365	0.231	0.217
R^2	0.9693	0.9497	0.9213	0.8238	0.7016
Pseudo-second-order rate model					
q_e	0.0381	0.0672	0.0777	0.0975	0.1011
k2	17.64	18.56	17.73	16.93	17.66
R^2	0.9984	0.9970	0.9983	0.9991	0.9985
Elovich model					
α	0.0628	0.1882	0.3228	0.9709	2.1231
β	131.96	76.64	72.66	69.53	76.79
R^2	0.9679	0.8887	0.8591	0.8554	0.9334
Intra-particle diffusion model					
I	0.0091	0.0241	0.0324	0.0487	0.0546
K_{id}	0.0076	0.0124	0.0130	0.0138	0.0129
R^2	0.8462	0.7091	0.6743	0.6873	0.8076

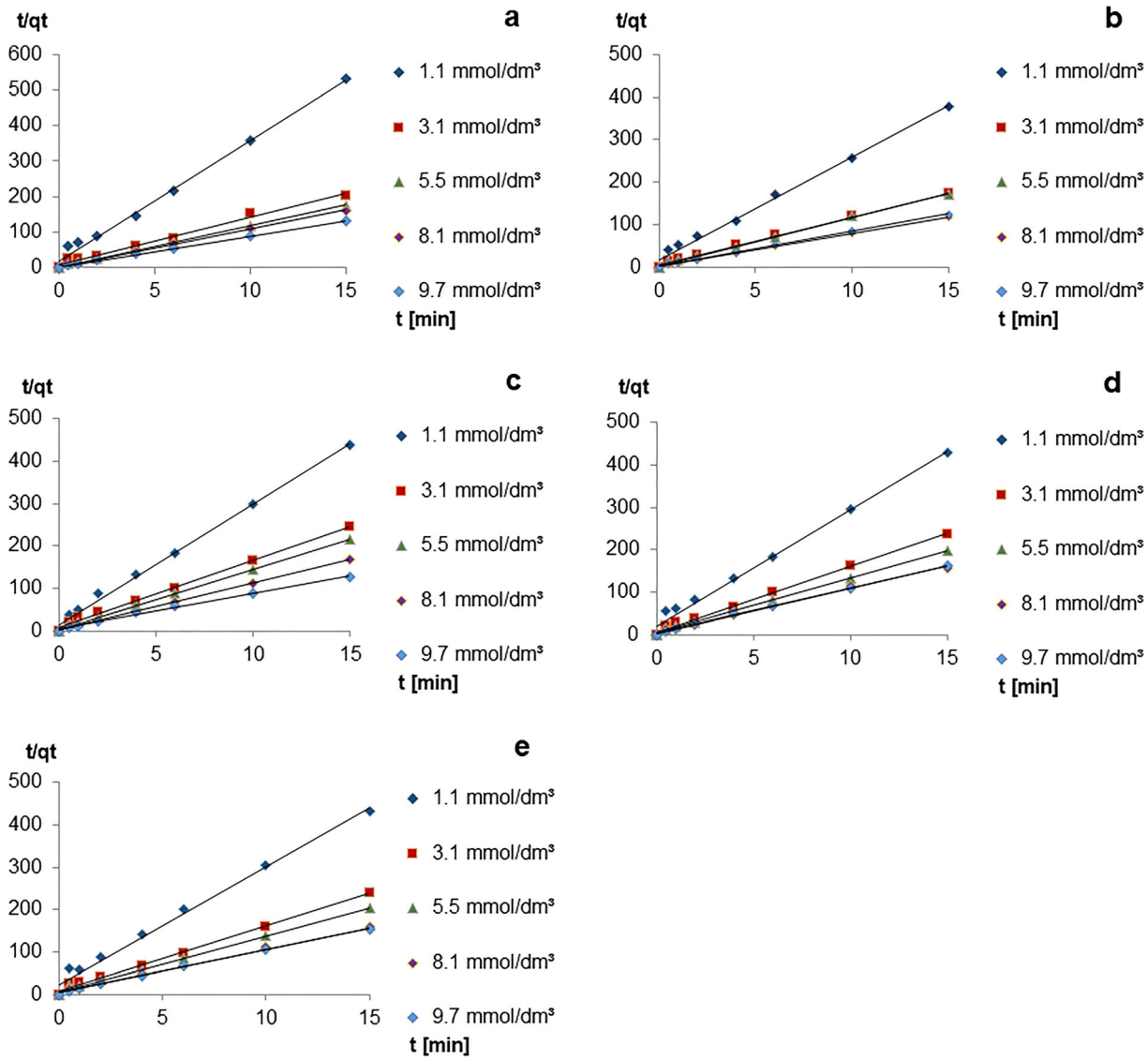

Fig. 7 Line graphs of pseudo-second order model of sorption kinetics for ammonium: **a** UM, **b** NaCl 3 h, **c** NaCl 54 h, **d** $NaNO_3$ 17 h, **e** K_2SO_4 16 h

capacity. For the lowest ammonium concentration, an increase in sorption capacity was observed for all modifications. The highest increase in sorption capacity was observed for 3-h modification with NaCl, which was equal to 28%. For other modifications, it was average 18–19%. At concentrations of 3 and 5 mmol/dm^3, an increase in sorption capacity was observed only on material modified with NaCl for 3 h (~15% and ~2.5%). For the remaining modifications, the sorption capacity was reduced by 17–19% for 3 mmol/dm^3 and 12–22% for 5 mmol/dm^3, respectively. At a concentration of 7 mmol/dm^3, an increase in sorption capacity was observed for three modifications by ~27% (NaCl 3 h), ~1.5% ($NaNO_3$), and ~0.5% (K_2SO_4). However, for a concentration of 9 mmol/dm^3, an increase in sorption capacity was observed for NaCl modification, ~6.5% for 3 h and ~4.5% for 24 h. Material modified with $NaNO_3$ and K_2SO_4 decreased in its sorption capacity by ~21% and 14.5%. During the study, it was observed that the rate of reaching equilibrium between the bed and ammonium ions changed. For unmodified material, equilibrium was reached after 4 min for concentration equal to 1 and 3 mmol/dm^3,

and for 5–9 mmol/dm^3 after 6 min. In the case of NaCl modification for 3 h, equilibrium time was reached after 4 min for all tested concentrations. Other modifications resulted in equilibrium being reached after 6 min at all concentrations tested.

The most faithful mathematical description of the sorption kinetics of ammonia on *raphia* provides a pseudo-second-order model. The R^2 determination coefficient for all sorbent types and the entire range of concentrations tested is at least 0.9955 for this model. On this basis, it can be assumed that sorption of ammonia on *raphia* is of chemical nature (Ho 2006).

Figure 7 presents graphical interpretations of the sorption kinetics model for particular types of sorbent. One can notice a high adjustment of the measurement data to the pseudo-second-order model.

4 Conclusion

The research confirms that *raphia* sp. fibers can be used as a biosorbent to remove ammonia from water. The sorption capacity of raphia in relation to ammonia ranges from 0.093 mmol/g for $NaNO_3$-modified *raphia* to 0.121 mmol/g for NaCl-modified *raphia* for 3 h. The ammonia removal rate for unmodified *raphia* for concentrations of 5, 7, and 9 mmol/dm^3 is equal to 24, 17, and 17%, while for concentrations of 1 and 3 mmol/dm^3 equal to 42% and 51%, respectively. The highest increase in the removal of ammonia from the model solution relative to *raphia* with unmodified surface was observed for modification of the *raphia* surface using NaCl for 3 h. At the lowest initial concentration, 1 mmol/dm^3, the degree of ammonia removal increased by 60%, while for the highest initial concentration, 9 mmol/dm^3, increased by 8%. The Freundlich sorption equilibrium model best describes the sorption of ammonia on all types of sorbent used (R^2 equal to at least 0.9248), but the other models (Langmuir, Temkin, D-R) also correspond to the experimental data to a satisfactory degree (R^2 equal to at least 0.8706). The kinetics of ammonia sorption from the model sewage on unmodified *raphia* and all types of surface modification is best described by the pseudo-second-order sorption kinetics model (R^2 coefficient is at least equal to 0.9964). On this basis, it can be concluded that the adsorption is of chemical nature.

References

Abdelnaeim, M. Y., El Sherif, I. Y., Attia, A. A., Fathy, N. A., & El-Shahat, M. F. (2016). Impact of chemical activation on the adsorption performance of common reed towards cu(II) and cd(II). *International Journal of Mineral Processing, 157*, 80–88.

Alberdi, O., Arriaga, H., Calvet, S., Estellés, F., & Merino, P. (2016). Ammonia and greenhouse gas emissions from an enriched cage laying hen facility. *Biosystems Engineering, 144*, 1–12.

Appl, M. (1999). *Ammonia, 1. Introduction*. KGaA: Wiley-VCH Verlag GmbH and Co.

Araújo, C. S. T., Almeida, I. L. S., Rezende, H. C., Marcionilio, S. M. L. O., Léon, J. J. L., & de Matos, T. N. (2018). Elucidation of mechanism involved in adsorption of Pb(II) onto Lobeira fruit (Solanum lycocarpum) using Langmuir, Freundlich and Temkin isotherms. *Microchemical Journal, 137*, 348–354.

Azimi, B., Tahmasebpoor, M., Sanchez-Jimenez, P. E., Perejon, A., & Valverde, J. M. (2019). Multicycle CO2 capture activity and fluidizability of Al-based synthesized CaO sorbents. *Chemical Engineering Journal, 358*, 679–690.

Azizian, S., Eris, S., & Wilson, L. D. (2018). Re-evaluation of the century-old Langmuir isotherm for modeling adsorption phenomena in solution. *Chemical Physics, 513*, 99–104.

Bhardwaj, N., & Bhaskarwar, A. N. (2018). A review on sorbent devices for oil-spill control. *Environmental Pollution, 243*, 1758–1771.

Bispo, M. D., Schneider, J. K., Silva Oliveira, D., Tomasini, D., Silva Maciel, G. P., Schena, T., et al. (2018). Production of activated biochar from coconut fiber for the removal of organic compounds from phenolic. *Journal of Environmental Chemical Engineering, 6*, 2743–2750.

Chwastowski, J., Staroń, P., Kołoczek, H., & Banach, M. (2017). Adsorption of hexavalent chromium from aqueous solutions using Canadian peat and coconut fiber. *Journal of Molecular Liquids, 248*, 981–989.

Coles, C. A., & Yong, R. N. (2002). Aspects of kaolinite characterization and retention of Pb and cd. *Applied Clay Science, 22*, 39–45.

Conley, D. J., Paerl, H. W., Howarth, R. W., Boesch, D. F., Seitzinger, S. P., Havens, K. E., Lancelot, C., & Likens, G. E. (2009). ECOLOGY controlling eutrophication: Nitrogen and phosphorus. *Science, 323*, 1014–1015.

Cui, X., Hao, H., Zhang, C., He, Z., & Yang, X. (2016). Capacity and mechanisms of ammonium and cadmium sorption on different wetland-plant derived biochars. *Science of the Total Environment, 539*, 566–575.

Długosz, O., & Banach, M. (2018a). Kinetic, isotherm and thermodynamic investigations of the adsorption of Ag+ and Cu2+ on vermiculite. *Journal of Molecular Liquids, 258*, 295–309.

Długosz, O., & Banach, M. (2018b). Sorption of Ag+ and Cu2+ by vermiculite in a fixed-bed column: Design, process optimization and dynamics investigations. *Applied Sciences, 8*, 2221.

Guo, X., & Wang, J. (2019). A general kinetic model for adsorption: Theoretical analysis and modeling. *Journal of Molecular Liquids, 288*, 111100.

Henry, J., & Aherne, J. (2014). Nitrogen deposition and exceedance of critical loads for nutrient nitrogen in Irish grasslands. *Science of the Total Environment, 470-471*, 216–223.

Ho, Y. S. (2006). Review of second-order models for adsorption systems. *Journal of Hazardous Materials, B136*, 681–689.

Hu, Y., Liu, W., Yang, Y., Qu, M., & Li, H. (2019). CO_2 capture by Li_4SiO_4 sorbents and their applications: Current developments and new trends. *Chemical Engineering Journal, 359*, 604–625.

Huang, J., Chen, J., Xie, Z., & Xu, X. (2015). Treatment of nanofiltration concentrates of mature landfill leachate by a coupled process of coagulation and internal microelectrolysis adding hydrogen peroxide. *Environmental Technology, 36*, 1001–1007.

Hunt, A. M. W., & Speakman, R. J. (2015). Portable XRF analysis of archaeological sediments and ceramics. *Journal of Archaeological Science, 53*, 626–638.

Inyang, H. I., Onwawoma, A., & Bae, S. (2016). The Elovich equation as a predictor of lead and cadmium sorption rates on contaminant barrier minerals. *Soil and Tillage Research, 155*, 124–132.

Jorgensen, T. C., & Weatherley, L. R. (2003). Ammonia removal from wastewater by ion exchange in the presence of organic contaminants. *Water Research, 37*, 1723–1728.

Lin, L., Lei, Z., Wang, L., Liu, X., Zhang, Y., Wan, C., Lee, D.-J., & Tay, J. H. (2013). Adsorption mechanisms of high-levels of ammonium onto natural and NaCl-modified zeolites. *Separation and Purification Technology, 103*, 15–20.

Milonji, S., Bispo, I., Fedoroff, M., Loos-Neskovic, C., & Vidal-Madjar, C. (2002). Sorption of cesium on copper hexacyanoferrate/polymer/silica composites in batch and dynamic conditions. *Journal of Radioanalytical and Nuclear Chemistry, 252*, 497–501.

Petit, S., Righi, D., & Madejová, J. (2006). Infrared spectroscopy of NH_4^+-bearing and saturated clay minerals: A review of the study of layer charge. *Applied Clay Science, 34*, 22–30.

Shalini, S. S., & Joseph, K. (2012). Nitrogen management in landfill leachate: Application of Sharon, Anammox and combined Sharon-Anammox process. *Waste Management, 32*, 2385–2400.

Šiljeg, M., Foglar, L., & Kukučka, M. (2010). The ground water ammonium sorption onto Croatian and Serbian clinoptilolite. *Journal of Hazardous Materials, 178*, 572–577.

Simonin, J. P. (2016). On the comparison of pseudo-first order and pseudo-second order rate laws in the modeling of adsorption kinetics. *Chemical Engineering Journal, 300*, 254–263.

Staroń, P., Chwastowski, J., & Banach, M. (2017). Sorption and desorption studies on silver ions from aqueous solution by coconut fiber. *Journal of Cleaner Production, 149*, 290–301.

Veliscek-Carolan, J., Thorogood, G. J., Gregg, D. J., Tansu, M., & Hanley, T. L. (2019). Ceramic conversion and densification of zirconium phosphonate sorbent materials. *Journal of Nuclear Materials, 516*, 327–334.

Veneu, D. M., Yokoyama, L., Cunha, O. G. C., Schneider, C. L., & de Mello Monte, M. B. (2018). Nickel sorption using Bioclastic granules as a sorbent material: Equilibrium, kinetic and characterization studies. *Journal of Materials Research and Technology, 209*, 684–697.

Xu, Y., Ding, H., Luo, C., Zheng, Y., Xu, Y., Li, X., Zhang, Z., Shen, C., & Zhang, L. (2018). Effect of lignin, cellulose and hemicellulose on calcium looping behavior of CaO-based sorbents derived from extrusion-spherization method. *Chemical Engineering Journal, 334*, 2520–2529.

Zhang, T., Ding, L., & Ren, H. (2009). Pretreatment of ammonium removal from landfill leachate by chemical precipitation. *Journal of Hazardous Materials, 166*, 911–915.

Zhu, Q., Moggridge, G. D., & D'Agostino, C. (2016). Adsorption of pyridine from aqueous solutions by polymeric adsorbents MN 200 and MN 500. Part 2: Kinetics and diffusion analysis. *Chemical Engineering Journal, 306*, 1223–1233.